BRAIN
ORIGINAL ARTICLE

CXCR3-mediated natural killer cell infiltration exacerbates white matter injury after intracerebral haemorrhage

Anson C. K. Ng,[1] Cuiting Zhang,[1] Tsz Lung Lam,[1] Karrie M. Kiang,[1] Vaness N. C. Ng,[2] Zhiyuan Zhu,[1,3] Jiaxin Liu,[1] Wenwei Tu,[4] Wanjun Tang,[1] Katrina C. W. Chau,[1] Kwan Man[1] and Gilberto K. K. Leung[1,5]

Intracerebral haemorrhage (ICH), a subtype of stroke, carries a grim prognosis. The inflammatory response during the early phase of ICH is a major perpetuator of neurological damage. Recent clinical studies suggest possible participation of the CXC chemokine receptor 3 (CXCR3)–chemokine system in mediating neuroimmune crosstalk, which exacerbates neurological dysfunction and might serve as a potential therapeutic target in the management of ICH. CXCR3 is expressed by natural killer (NK) cells, which are known to be pathogenic in ICH. However, whether and how CXCR3 promotes NK cell infiltration and functioning in ICH and whether the attenuation of CXCR3 might affect neurological outcome have not been delineated. The present preclinical study has demonstrated, for the first time, the role of CXCR3 in facilitating the ingress of NK cells from the systemic compartment into the haemorrhagic brain and in causing ICH-related neurological injury.

CXCR3 expression was found to be upregulated in the peri-haematomal region including the white matter tracts, with CXCR3+ leucocytes being the main contributor. When compared with wild-type mice, CXCR3 knockout mice showed splenic pooling of NK cells, suggestive of impaired systemic recruitment. Adoptive intravenous transfer of NK cells obtained from wild-type mice resulted in significantly greater cerebral homing of NK cells than after the transfer of NK cells obtained from CXCR3 knockout mice, confirming the pivotal role of CXCR3. Global CXCR3 deficiency was associated with reduced recruitment of NK cells expressing interferon-gamma (IFN-γ), the prototypic cytokine responsible for NK cell-induced inflammatory responses, in addition to better corticospinal tract integrity in the cervical spinal cord and improved neurological outcomes in terms of gross and fine motor functions. Systemic administration of AMG487, a CXCR3 antagonist, achieved the same effects.

In conclusion, CXCR3, NK cells and IFN-γ operate in concert in ICH pathogenesis, and the attenuation of CXCR3 has important translational potential. Our findings present a new research direction in identifying novel strategies for mitigating the detrimental neuroinflammatory responses found in ICH and, possibly, in other neurological conditions.

1 Department of Surgery, School of Clinical Medicine, LKS Faculty of Medicine, The University of Hong Kong, Hong Kong SAR 999077, China
2 The Royal Veterinary College, University of London, London NW1 0TU, UK
3 Department of Functional Neurosurgery, Zhujiang Hospital, Southern Medical University, Guangzhou 510000, China
4 Department of Paediatrics and Adolescent Medicine, School of Clinical Medicine, LKS Faculty of Medicine, The University of Hong Kong, Hong Kong SAR 999077, China
5 The State Key Laboratory of Brain and Cognitive Sciences, The University of Hong Kong, Hong Kong SAR 999077, China

Correspondence to: Gilberto Ka Kit Leung
Department of Surgery, School of Clinical Medicine, LKS Faculty of Medicine
The University of Hong Kong, Queen Mary Hospital
102 Pokfulam Road, Pokfulam, Hong Kong SAR 999077, China
E-mail: gilberto@hku.hk

Introduction

Recent discoveries concerning neuroimmunological crosstalk offer new insights into the management of intracerebral haemorrhage (ICH).[1] Multiple immune cell types participate in different pathological phases of ICH,[2-5] and their manipulations could reduce secondary brain damage to favour neurological recovery.[5,6] Although the neuroinflammatory role of leucocytes of the myeloid lineage has been studied extensively in ICH,[6-10] much less is known about the role of lymphoid cells, particularly that of natural killer (NK) cells.[11,12] NK cells abound within the peri-lesional region of ICH at an early stage, outnumbering other peripheral leucocyte populations and coinciding with the commencement of critical pathological events including brain oedema, neuroinflammation and white matter injury.[5,13] Furthermore, the initial peri-lesional milieu favours the activation of NK cells via the expression of activating ligands induced by cell stress and cytokines.[12,14,15] Based on these observations, NK cells have been proposed to be the early responders that orchestrate secondary brain injury through cytokine secretion and cytotoxicity to susceptible cells,[5] and whole-body depletion of NK cells has been found to improve neurological functions in mice.[16] Although such treatment is infeasible in human subjects, the specific inhibition of NK cell infiltration is a potential viable alternative.

Immune cell trafficking involves multiple components, one of which is the CXC chemokine receptor (CXCR) system that acts as a bridge between the systemic and brain compartments through the binding of chemokines released from the lesion site to chemokine receptors on immune cells.[17,18] Distinct chemokine receptors are expressed by specific leucocytes.[8,9,19] Among these, CXCR3 expressed by NK cells is responsible for their recruitment to pathological sites, including the ischaemic brain.[20-22] CXCR3 ligands are highly expressed in the peri-haemorrhagic brain regions in mice,[5] and the upregulation of CXC motif chemokine ligand 10 (CXCL10), a CXCR3 ligand, is associated with poorer clinical outcomes after ICH,[23] suggesting that CXCR3 might be a potential therapeutic target.

The aim of the present study was to investigate the role of CXCR3 in mediating the NK cell response in ICH and to assess the therapeutic benefits of CXCR3 inhibition. For the first time, we demonstrate that CXCR3 facilitates the homing of a subset of NK cells to the haemorrhagic brain and that CXCR3 inhibition could mitigate white matter injury and promote neurological recovery. Our findings provide a scientific foundation for future clinical translation, in light of the fact that several classes of CXCR3 antagonists are already available for research use.[24]

Materials and methods
Experimental animals

All experimental protocols were approved by the Committee on the Use of Live Animals in Teaching and Research (CULATR) of our institution. Twelve- to 14-week-old male wild-type C57BL/6 mice (WT mice), CXCR3 knockout mice (CXCR3-KO mice) on a C57BL/6 background[25] and Rag2$^{-/-}$γc$^{-/-}$ mice[26] were used. Male mice were used to rule out the potential hormonal effect and the influence of biallelic expression of CXCR3 in biological female mice[27] on ICH outcomes. The animals, weighing between 21 and 31 g, were habituated at the same animal unit for ≥7 days after being transferred from the Centre for Comparative Medicine Research (CCMR) of our institution to reduce stress. All were kept in a 12 h–12 h light–dark cycle with enrichment and *ad libitum* access to water and chow. The animal holding room was kept at 19°C ± 2°C, with humidity maintained at 44% ± 2%.

Animal model

ICH was induced in the morning, as described previously by our group, with slight modifications.[28] A burr hole was created 0.2 mm anterior to bregma and 2 mm lateral to the midline on the right side of the skull. A 26-gauge Hamilton syringe (10 μl) (Hamilton) filled with 0.5 μl of 0.08 U/μl type IV bacterial collagenase (C5138; Sigma-Aldrich) in 0.9% normal saline was placed into the right striatum, with the tip of the needle 3.5 mm deep to the dura. Collagenase was injected at 0.175 μl/min. The sham group underwent surgery with needle insertion only.

CXCR3 inhibition

WT mice were randomly assigned to receive the CXCR3 inhibitor AMG487 (HY-15319; MedChemExpress) or vehicle. AMG487 was dissolved in 100% ethanol at 50 mg/ml and diluted to 2.5 mg/ml using PBS with 10% Tween-80 (HY-Y1891; MedChemExpress). The working solution (30 mg/kg) was injected intraperitoneally 2 h after ICH induction, and then twice daily for 7 days. The control group received only the drug vehicle. The treatment regimen was modified from several clinical and preclinical studies and our own preliminary study.[29-31]

Motor function assessment

Post-ICH functional recovery was assessed by three behavioural tests performed in the morning by independent researchers blinded to the experimental groups. The sequence of testing was the cylinder test, followed by the accelerated rotarod, then the grid-walking test.

Cylinder test

This was conducted as described previously, with slight modifications.[32] A push-off from the cylinder wall during rearing was regarded as an independent use of one forelimb or simultaneous use of both forelimbs. Each mouse was observed for 10 min or for 20 contacts with the wall within 10 min. Mice that made <10 wall contacts were excluded from the analysis, because this was

considered an unreliable measure of forelimb use. The percentage of spontaneous impaired forelimb usage was calculated as:

$$\frac{\text{Total number of impaired limb usage} + \left(\frac{1}{2}\right) \text{number of both limb usage}}{\text{Total number of wall contacts}} \times 100\%$$

(1)

Accelerated rotarod test

This was conducted as described previously, with slight modifications.[32] The accelerating condition ranged from 4 to 40 rotations/min over 5 min. The latency to fall from the rotating rod was recorded (maximum value: 300 s). Average latency to fall was calculated by averaging the data generated from three trials.

Grid walking test

The mice were placed on a 30 cm × 44 cm wire rectangular grid containing 13 mm × 13 mm grid squares 50 cm above the floor. A foot fault was defined as either missing the rung completely by the paw such that the limb fell from the rungs and the animal lost balance or as placing the paw correctly on the rung but slipping off during weight bearing. The mice were allowed to explore freely for 5 min. The percentage of foot fault was calculated as:

$$\frac{\text{Number of foot faults observed for the impaired forelimb}}{\text{Total steps taken by the impaired forelimb}} \times 100\%$$

(2)

Tissue preparation for cryosections

Mice were anaesthetized in the morning with pentobarbital sodium (200 mg/kg, intraperitoneally) on Day 7 post-ICH and post-sham operation, followed by transcardial perfusion with 40 ml of ice-cold phosphate buffered saline (PBS, pH = 7.4) and 4% (w/v) paraformaldehyde (158127; Sigma-Aldrich) in 0.1 M PBS. The brains were harvested and fixed in 4% paraformaldehyde at 4°C overnight. A sucrose gradient (10%, 20% and 30%, w/v, in 1× PBS, sequentially) was used to dehydrate the brain samples at 4°C (S5016; Sigma-Aldrich).

Immunofluorescence staining

Three coronal brain sections (10-µm-thick cryosections) of each brain sample were randomly selected among the slides with haematoma. Imaging of fluorescently labelled frozen brain sections was performed using LSM 800 confocal microscope with airyscan module (Carl Zeiss). The 20× and 40× with oil immersion objective lenses were used. Random non-overlapping images for each brain section were acquired from the peri-haematomal region, defined as the 1-mm-wide region surrounding the haematoma,[33] using the same imaging setting. Primary and secondary antibodies used are listed in the Supplementary material.

Luxol Fast Blue staining and quantification of white matter loss

Three coronal brain sections (10-µm-thick cryosections) of each brain sample with the haematoma were randomly selected. Myelin staining was performed using a Luxol Fast Blue (LFB) stain kit (ab150675; Abcam). Whole brain sections were imaged using Vectra Polaris (Akoya Biosciences) and a DP74 colour fluorescence camera (Olympus) using a 10× objective. The region of demyelination in the ipsilateral striatum was indicated by lack of LFB stain, i.e. a pale area. ImageJ software was used to measure the hemispheric area and the area of demyelination after manually tracing the borders of the targeted regions of each section (ImageJ, US National Institutes of Health, Bethesda, MD, USA, https://imagej.net/ij/, 1997–2018). The area of demyelination was expressed as a percentage of the cross-sectional hemispheric area.

Transmission electron microscopy

Mice were sacrificed using the same method stated above. All samples were collected at 7 days post-ICH or post-sham surgery. Samples were prepared for microscopic analysis as described previously, with slight modifications.[28] The sections were photographed at ×1200 and ×3900 using a CM100 transmission electron microscope (Philips). Quantification was done by methods described previously, with slight modifications.[34] In addition, three non-overlapping regions (464 µm² each) within the contralesional dorsal corticospinal tract (CST) in the C5 segment of the cervical spinal cord were randomly selected. Around 1000 axons, including all the healthy, demyelinated and degenerated axons, were counted for each sample. Quantifications of demyelinated axons and degenerated axons were expressed as percentages of the total number of axons per section. The number of excessive myelin figures was counted in each section.

RT-qPCR

Mice were sacrificed, transcardially perfused, and their brains harvested and cut into 2-mm-thick coronal sections. The cortex was removed from the hemispheres and discarded, leaving the corpus callosum and striatum intact. The tissue samples (haematoma, striatum and corpus callosum) were snap-frozen in liquid nitrogen and stored at −80°C until use. RT-qPCR was performed as previously described.[35] Briefly, RNA transcript extracts were reverse transcribed into complementary DNA by reverse transcriptase. The complementary DNA was amplified by PCR and quantified by measuring the fluorescence signal. The mRNA expression levels of the genes of interest were normalized to that of the housekeeping gene GAPDH. The $2^{-\Delta\Delta Ct}$ method was used to calculate relative gene expression levels. The relative expression levels of all genes of interest in the sham group were normalized to one. Primer sequences used are listed in the Supplementary material.

Flow cytometry

Flow cytometry was done as described previously, with slight modifications.[36] Mice were sacrificed 1 day after the sham procedure or on Day 1, 3 or 7 post-ICH using the same method as above. The spleens were collected before transcardial perfusion using 40 ml of ice-cold PBS. The cerebral hemispheres were separated, then homogenized mechanically and enzymatically with 1 ml of accutase (A1110501; Gibco, Thermo Fisher Scientific) for 15 min and put through 70 µm cell strainers using syringe plungers.[32,37] The pellets were resuspended in a 30% Percoll gradient (GE17-0891-02; Sigma-Aldrich) to remove myelin sheaths and debris. Leucocytes were enriched in the cell pellets and used for subsequent staining with or without stimulation. The spleens were homogenized and prepared as described previously.[36] All procedures were carried out at room temperature unless otherwise specified. Antibodies and dyes used are listed in the Supplementary material. Compensation and sample acquisition were performed using NovoCyte Quanteon and Advanteon (Agilent). Data analysis was done using NovoExpress software (v.1.4.1; Agilent). The gating strategies were determined by fluorescence minus one control. Contour plots were used for illustration.

Ex vivo stimulation of cells for intracellular cytokine detection

Single-cell suspensions generated from mouse brains in complete RPMI-1640 medium were stimulated with 100 ng/ml phorbol 12-myristate 13-acetate (P8139; Sigma-Aldrich) and 500 ng/ml ionomycin (I9657; Sigma-Aldrich). The mixtures were incubated simultaneously with the cell transporter inhibitor brefeldin A (00-4506-51; eBioscience, Invitrogen, Thermo Fisher Scientific) for 4 h at 37°C. Negative controls were incubated with brefeldin A without stimulants for 4 h at 37°C. Cells were stained with Zombie Violet dye and antibodies as previously described and according to the manufacturer's protocol.[32,38]

Natural killer cell enrichment and adoptive transfer

Spleens from healthy WT and CXCR3-KO mice were harvested and homogenized as described previously.[39] NK cells were isolated using the MojoSort™ Mouse NK Cell Isolation Kit (480050; Biolegend). More than 75% of the cells isolated were NK cells, as determined by flow cytometry (Supplementary Fig. 1). All Rag2$^{-/-}$γc$^{-/-}$ mice received 5×10^5 NK cells 3 days post-ICH intravenously under inhaled anaesthesia. The brains of the recipient mice were harvested 4 days post-injection for flow cytometry analysis.

Statistical analysis

Data are shown as the mean ± standard error of the mean (SEM). Animals were all assigned randomly to experimental groups by researchers blinded to the experimental conditions, which were determined by a researcher not involved in the conduct of experiments, outcome assessment and data analysis. Mice were excluded if they died postoperatively before experimental end points ($n = 4$ for WT ICH group, $n = 1$ for CXCR3-KO ICH group, $n = 1$ for vehicle group and $n = 2$ for AMG487 group). The sample size was mainly determined with reference to previous studies and our own preliminary studies. Cohen's formulae (Cohen's *d* for comparison of two groups and Cohen's *f* for multiple group comparisons) were used to calculate the effect size. G*Power v.3.1.9.7 was used for power analysis.[40] Statistical difference in the means between two groups was tested with Student's two-tailed unpaired *t*-test (with Welch's correction or the Mann–Whitney modification). One-way ANOVA or two-way ANOVA followed by *post hoc* Tukey's multiple comparisons test, Dunnett's multiple comparisons test or Šídák's multiple comparisons test were used to compare means of three or more groups. A value of $P < 0.05$ was set as the cut-off for statistical significance. GraphPad Prism (v.9.3.1) software was used for statistical analysis (GraphPad Software, San Diego, CA, USA; www.graphpad.com). SPSS (v.27) was used to assess normality, sphericity and homogeneity of variances of the datasets (IBM SPSS Statistics for Windows, v.27.0, Released 2020; IBM Corp., Armonk, NY, USA).

Results

CXCR3 and CXCL10 expressions are upregulated in the haemorrhagic hemisphere

Progressive *CXCR3* mRNA upregulation relative to the sham group was observed starting from Day 3 post-ICH ($P < 0.05$ on Days 3 and 7 versus sham; $P > 0.05$ on Day 1 versus sham; Fig. 1A). *CXCR3* expression in the contralateral hemisphere without ICH was unchanged at all time points (Fig. 1B). Needle insertion itself did not affect *CXCR3*

expression ($P > 0.05$ left hemisphere versus right hemisphere with needle insertion; Fig. 1C), indicating that ICH was the cause of *CXCR3* upregulation within the lesioned hemisphere. Given that CXCL10 has been shown clinically to be associated with poorer ICH outcomes, its expression was also measured. Upregulation of *CXCL10* expression preceded that of *CXCR3* during the acute phase ($P < 0.01$ on Days 1 and 7 versus sham; $P > 0.05$ on Day 3 versus sham; Fig. 1D).

To identify the cell source of CXCR3, cells from the hemorrhagic hemisphere were co-stained with the haematopoietic marker CD45 and CXCR3. CD45^{hi} leucocytes were the main population expressing CXCR3 throughout the first week post-ICH (Fig. 1E). Very few CD45^{int} microglia and CD45$^-$ cells (including neurons, astrocytes, cells of oligodendroglial lineages and endothelial cells) showed co-staining, indicating that CXCR3$^+$ CD45^{hi} leucocytes were the main contributors to the rise in CXCR3 expression. The number of CXCR3$^+$ NK cells increased significantly starting from Day 3 post-ICH compared with sham ($P < 0.05$ on Days 3 and 7 versus sham; $P > 0.05$ on Day 1 versus sham; Fig. 1F). This was probably attributable to increased accumulation rather than on-going haemorrhage, because there was no evidence of haematoma enlargement (Supplementary Fig. 2). Interestingly, the mean fluorescent level (MFI) of CXCR3 on NK cell surfaces decreased at all time points ($P < 0.05$ at all time points post-ICH versus sham; Fig. 1F), pointing towards a drop in cell surface expression of CXCR3 despite gradual NK cell accumulation, which could be attributable to active ligand binding to CXCR3 on NK cells causing internalization of the complex.

Natural killer cell accumulation is mediated by CXCR3 after ICH

We then examined the role of CXCR3 in NK cell recruitment using CXCR3-KO mice. Sham operation did not result in statistically significant differences in the number of NK cells between WT and CXCR3-KO mice ($P > 0.05$ WT sham versus CXCR3-KO sham; Fig. 2A). ICH induced a significant increase in the number of NK cells in WT mice ($P < 0.01$ WT sham versus WT ICH; Fig. 2A), but not in CXCR3-KO mice on Day 7 ($P < 0.001$ WT ICH versus CXCR3-KO ICH; Fig. 2A). No significant differences were found between CXCR3-KO sham brains and CXCR3-KO ICH brains ($P > 0.05$ CXCR3-KO sham versus CXCR3-KO ICH), indicating that CXCR3 depletion would completely suppress the accumulation of NK cells in the haemorrhagic hemisphere (Fig. 2A). Immunofluorescence staining showed that more NK cells were present in the peri-haematomal region of the WT brains, which could be CXCR3-positive (CXCR3$^+$) or -negative (CXCR3$^-$), whereas no CXCR3 signal was detected in the CXCR3-KO mice (Fig. 2B and Supplementary Fig. 3). NK cells were situated in the peri-haematomal region close to the white matter, which hinted at their involvement in white matter injury (Fig. 2C).

Additionally, we briefly examined the change in the interferon-gamma-positive (IFN-γ$^+$) NK cell population, because IFN-γ is the prototypic cytokine released by NK cells known to participate in CXCR3-mediated inflammatory responses. We found that the percentage of IFN-γ$^+$ NK cells was significantly lower in the CXCR3-KO group than in the WT group ($P < 0.001$ WT ICH versus CXCR3-KO ICH), implying that CXCR3 was indeed crucial for the accumulation of IFN-γ$^+$ NK cells and possibly their inflammatory effects (Fig. 2E). Measurement of MFI did not show significant differences in the intensity of intracellular IFN-γ expression after ICH induction, suggesting that those NK cells in the haemorrhagic hemisphere of CXCR3-KO mice retained the ability to express IFN-γ ($P > 0.05$ WT ICH versus CXCR3-KO ICH).
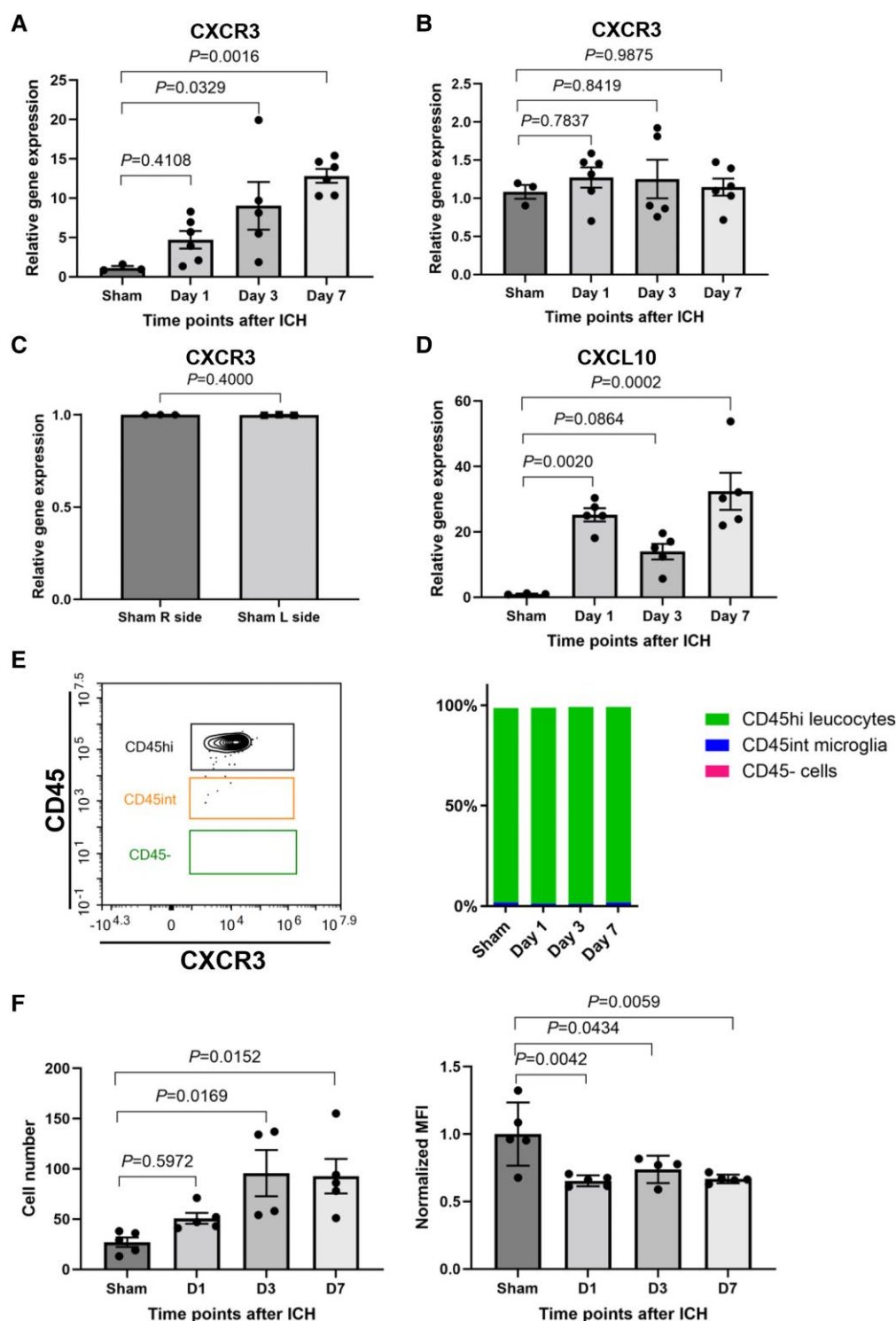
Figure 1 CXCR3 and CXCL10 expressions are upregulated in the haemorrhagic hemisphere. ICH was induced in WT C57BL/6 mice. (**A**) There was a significant increase in *CXCR3* mRNA expression in the haemorrhagic hemisphere starting from Day 3 relative to that of sham (Cohen's f = 1.08). (**B**) There were no significant changes in *CXCR3* gene expression in the contralateral hemisphere at all time points compared with sham (Cohen's f = 0.67). (**C**) Needle insertion did not alter *CXCR3* mRNA expression (Cohen's d = 1.37). (**D**) There was significant upregulation of *CXCL10* gene expression in the haemorrhagic hemisphere for ≥1 week post-ICH relative to that of sham (Cohen's f = 1.73). (**E**) Live CXCR3+ cells were further divided into CD45hi leucocytes, CD45int microglia and CD45− non-haematopoietic resident cells of the brain as shown in the flow cytometry plot based on the intensity of CD45 expression (high, intermediate or negative). CD45hi leucocytes consistently constituted the largest CXCR3-expressing population throughout the first week. (**F**) The number of CXCR3-expressing NK cells increased significantly starting from Day 3 post-ICH compared with sham (Cohen's f = 2.31). The relative MFI of CXCR3 expression by NK cells was significantly lower than that of the sham group at all time points post-ICH (Cohen's f = 1.029). All *P*-values shown indicate the difference between each time point and sham. n = 3 mice for sham, n = 4–6 mice for ICH time points. Data are presented as the mean ± standard error of the mean. Statistical analysis was determined by one-way ANOVA except for (**C**) which used Mann–Whitney U-test. CD45 = cluster of differentiation 45; CXCR3 = CXC chemokine receptor 3; CXCL10 = CXC motif chemokine ligand 10; D = day; hi = high; ICH = intracerebral haemorrhage; int = intermediate; L = left; MFI = mean fluorescence intensity; NK = natural killer; R = right; WT = wild-type.
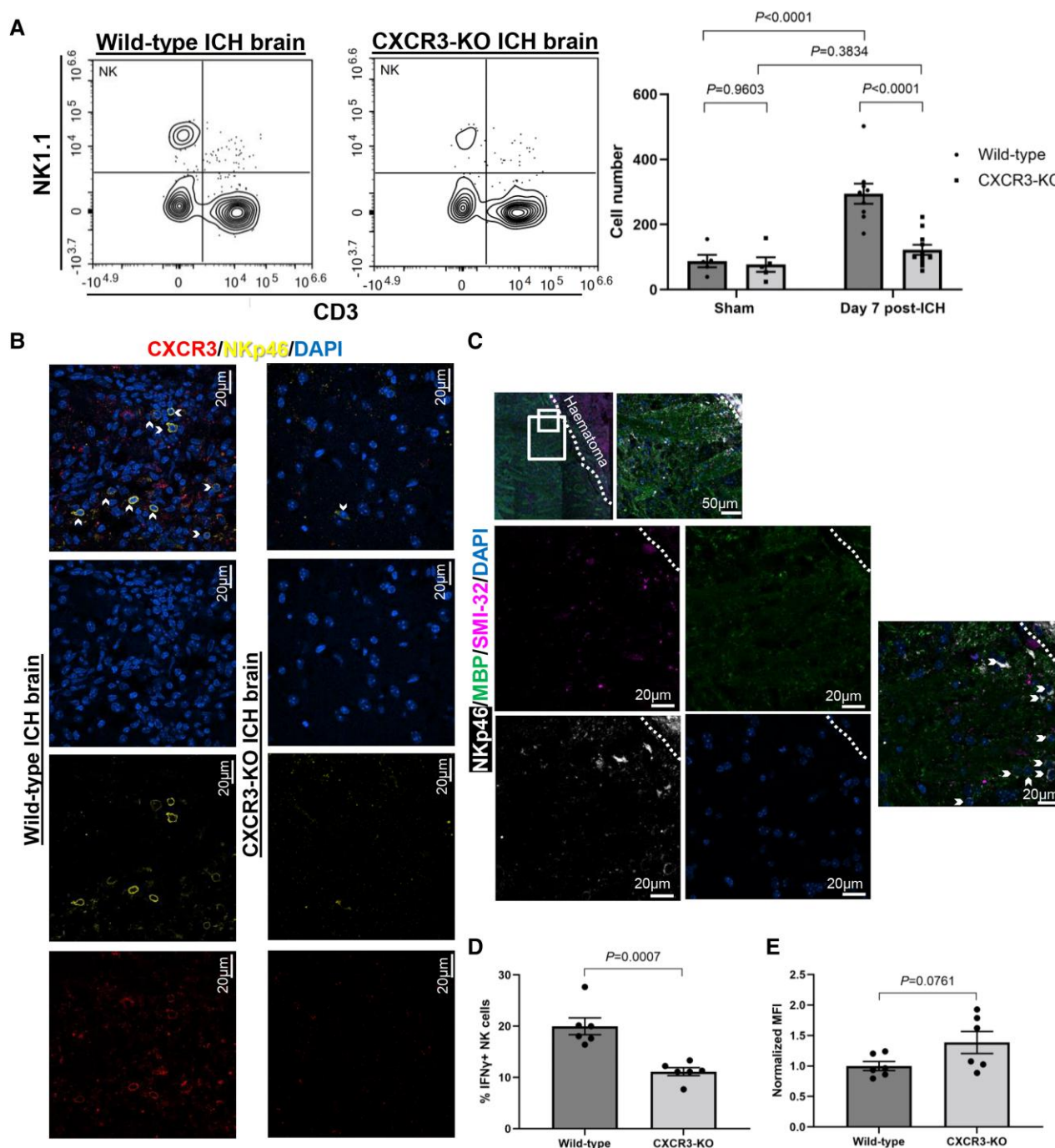
Figure 2 NK cell accumulation and IFN-γ expression are mediated by CXCR3 after ICH. (A) Flow cytometry plots showing subpopulations of CD45^{hi} leucocytes in the haemorrhagic hemisphere 7 days post-ICH, which were classified based on CD3 and NK1.1 surface expressions. There was a prominent rise in the number of NK cells from sham to Day 7 post-ICH in the WT group. Significantly fewer NK cells were detected in the CXCR3-KO group compared with the WT group on Day 7. There was no significant difference in the number of NK cells between the WT sham group and CXCR3-KO sham group or between the CXCR3-KO sham group and CXCR3-KO ICH group. $n = 5$ mice for sham groups, $n = 9$–11 mice for Day 7 ICH groups. Cohen's $f = 2.05$. Data are presented as the mean ± standard error of the mean (SEM). Statistical significance between was determined by two-way ANOVA with Šídák's multiple comparisons test. **(B)** Images of immunofluorescence staining of NKp46, CXCR3 and DAPI on the frozen brain section using a 40× objective lens. Both CXCR3$^+$ and CXCR3$^-$ NK cells were situated in the peri-haematomal region in WT mouse brain, but fewer NK cells were observed in CXCR3-KO mouse brain, which were all CXCR3$^-$. NKp46$^+$ cells are indicated by the white arrowheads. All images were taken randomly from the peri-haematomal region (within 1 mm from the edge of the haematoma). **(C)** Immunofluorescence staining of NKp46, MBP, SMI-32 and DAPI on the frozen brain section of WT ICH mice using a 20× or 40× objective lens. The NKp46$^+$ cells were located near the edge of the haematoma in close proximity to white matter, as indicated by the white arrowheads. The edge of the haematoma on each image is delineated by a white dotted line. All images were taken randomly from the peri-haematomal region, as indicated by the white frames. **(D)** Based on flow cytometry, the frequency of IFN-γ-expressing NK cells was significantly lower in the KO group 7 days after ICH (Cohen's $d = 3.30$). **(E)** No significant difference in MFI was observed for IFN-γ between WT and CXCR3-KO mice. $n = 6$ mice per group. Cohen's $d = 1.14$. Data are presented as the mean ± SEM. Statistical significance was determined by Student's two-tailed unpaired t-test. CD3 = cluster of differentiation 3; CXCR3 = CXC chemokine receptor 3; DAPI = 4′,6-diamidino-2-phenylindole; ICH = intracerebral haemorrhage; IFN-γ = interferon-gamma; KO = knockout; MBP = myelin basic protein; MFI = mean fluorescence intensity; NK = natural killer; NK1.1 = killer cell lectin-like receptor subfamily B member 1A; NKp46 = natural killer cell p46-related protein; SMI-32 = anti-neurofilament H (non-phosphorylated) antibody; WT = wild-type.

CXCR3 promotes recruitment of NK cells into haemorrhagic hemisphere from systemic compartment

NK cell accumulation in the haemorrhagic hemisphere could be attributable to local proliferation and/or ingress from the systemic compartment. Initially, we looked for any alteration in the systemic reservoirs, including the spleen and blood. A significantly higher splenic NK cell percentage was detected in the CXCR3-KO mice post-ICH ($P < 0.01$ WT spleen versus CXCR3-KO spleen; Fig. 3A). There were no corresponding changes in blood, which was not unexpected, because the number of NK cells in blood is time point sensitive and might not align with that in their natural reservoirs and the brain (Supplementary Fig. 4). The opposite trends of NK cell pooling between the spleen and the brain in CXCR3-KO mice were strongly suggestive of CXCR3-mediated recruitment. To confirm this, adoptive intravenous transfer of splenic NK cells from either WT or CXCR3-KO mice into $Rag2^{-/-}\gamma c^{-/-}$ mice, which lack NK cells was performed 3 days after ICH. No NK cells were detected in the $Rag2^{-/-}\gamma c^{-/-}$ mouse brain after ICH without adoptive transfer (Supplementary Fig. 5). The proportion of NK cells in the haemorrhagic hemisphere after adoptive transfer of WT NK cells was markedly higher than after transfer of CXCR3-KO NK cells on Day 7 post-ICH ($P < 0.05$ WT NK cell transfer versus CXCR3-KO NK cell transfer; Fig. 3B). This strongly supports the notion that CXCR3 is crucial for NK cell trafficking into the peri-haematomal region.

The association between CXCR3 and NK cell proliferation was examined. The percentage of Ki67$^+$ NK cells within the total NK cell population in the WT brains was not significantly higher than that in CXCR3-KO brains ($P > 0.05$ WT ICH versus CXCR3-KO ICH; Fig. 3C), suggesting that local proliferation was unlikely to account for the differences in the number of NK cells between WT and CXCR3-KO mice. However, we did not examine the direct effect of CXCR3 on NK cell proliferation.

Global CXCR3 deficiency attenuates neurological deficits and acute white matter injury

To uncover the significance of CXCR3-related immunomodulation, motor outcomes within the first week post-ICH were examined (Fig. 4A). Compared with WT mice, CXCR3-KO mice had significantly greater spontaneous impaired limb use ($P < 0.05$ WT ICH versus CXCR3-KO ICH at all time points; Fig. 4B) and a longer latency to fall from the rotating rod ($P < 0.05$ WT ICH versus CXCR3-KO ICH on Day 3, and $P < 0.01$ on Day 7; Fig. 4C), indicating a better preservation of gross motor functions in the presence of CXCR3 deficiency. Furthermore, left forelimb (the affected limb) usage by the CXCR3-KO mice showed a lower foot fault index relative to WT mice on Day 7 on the grid-walking test, which mainly assessed fine motor functions, including wireframe grasping and sensorimotor coordination ($P > 0.05$ WT ICH versus CXCR3-KO ICH on Day 3 and $P < 0.05$ on Day 7; Fig. 4D). No significant differences in survival and absolute body weight were observed between groups, suggesting that general health status was not significantly affected by systemic CXCR3 depletion (Supplementary Fig. 6).

It is known that the level of motor deficit is correlated with the degree of white matter injury after stroke.[41,42] Given that we found that NK cells were mainly located near the white fibre tracts (Fig. 2C), we proceeded to examine the possible effect of CXCR3 depletion on white matter injury on Day 7 post-ICH, when differences in motor performance between WT and CXCR3-KO mice were the greatest. Initially, LFB staining was used to identify areas of demyelination,

i.e. the loss of blue colour staining.[43] CXCR3-KO mouse brains had a significantly smaller percentage of demyelinated area ($P < 0.05$ WT ICH versus CXCR3-KO ICH; Fig. 4E). Immunofluorescence staining was then used to identify damage to the myelin sheaths and axons, signified by a reduction in MBP signal and an increase in SMI-32 intensity, respectively.[44-46] As shown in Fig. 4F, CXCR3-KO mice had better white matter structural integrity than did WT mice.

Changes in the CST are positively correlated with motor performance in stroke patients.[41] We examined alterations in myelin sheaths and axonal degeneration in the CST post-ICH using transmission electron microscopy.[28,47,48] The CST at C5 level of the spinal cord was chosen because: (i) the anatomical arrangement of the spinal cord allows easier identification of this long tract; and (ii) distal changes of the CST would reflect the extent of proximal injury in the subacute phase without being confounded by concomitant post-haemorrhagic histological changes.[49] Healthy white matter tracts at the C5 level from sham mice had axons that were uniform in size, with compact myelin sheaths (Fig. 4G), whereas injured CST at C5 level from ICH mice showed loosening of myelin lamellae, excessive myelin figures, axonal degeneration and swollen mitochondria (Fig. 4G). Such features were observed as soon as 7 days post-ICH. We found that the contralesional CST (carrying crossed fibres from the haemorrhagic striatum) of CXCR3-KO mice contained a significantly lower percentage of degenerating axons ($P < 0.001$ WT ICH versus CXCR3-KO ICH; Fig. 4H) and fewer excessive myelin figures ($P < 0.001$ WT ICH versus CXCR3-KO ICH; Fig. 4I). A reduction in the percentage of demyelinating axons was also observed in the CXCR3-KO group, although this did not reach statistical significance ($P > 0.05$ WT ICH versus CXCR3-KO ICH; Fig. 4J). Altogether, CXCR3 depletion was associated with better preservation of CST structural integrity.

Systemic CXCR3 antagonism by AMG487 improves outcomes of ICH

Lastly, we examined the effect of AMG487, an inhibitor of CXCR3. Consistent with the behavioural test results in CXCR3-KO mice, a milder degree of motor deficit was observed in WT mice treated with AMG487. The treatment group had a greater tendency to use the impaired limb, albeit without statistically significant differences ($P > 0.05$ vehicle versus AMG487 at all time points post-ICH; Fig. 5B). The treatment group spent a significantly longer period of time on the rotating rod than controls in the first week, reaching statistical significance on Day 7 ($P > 0.05$ vehicle versus AMG487 on Day 3; $P < 0.05$ vehicle versus AMG487 on Day 7; Fig. 5C). Grid walking also yielded significant results from Day 3 onwards, implying a better preservation of fine motor function in the treatment group ($P < 0.05$ vehicle versus AMG487 at all time points post-ICH; Fig. 5D). Importantly, the treatment group had a significantly smaller percentage of demyelination area compared with the vehicle group ($P < 0.05$ vehicle versus AMG487; Fig. 5E). AMG487 did not affect mortality rate or absolute body weight (Supplementary Fig. 7).

Discussion

Neurological damage in ICH was previously thought to be mainly attributable to mechanical injury, raised intracranial pressure and ischaemic insult, whereas recent findings also highlight the role of multiple immune cell types.[2-4] Li et al.[5] reported on the prominent role of NK cells in both patients and experimental animals, but the mechanism by which NK cells are recruited to the lesion
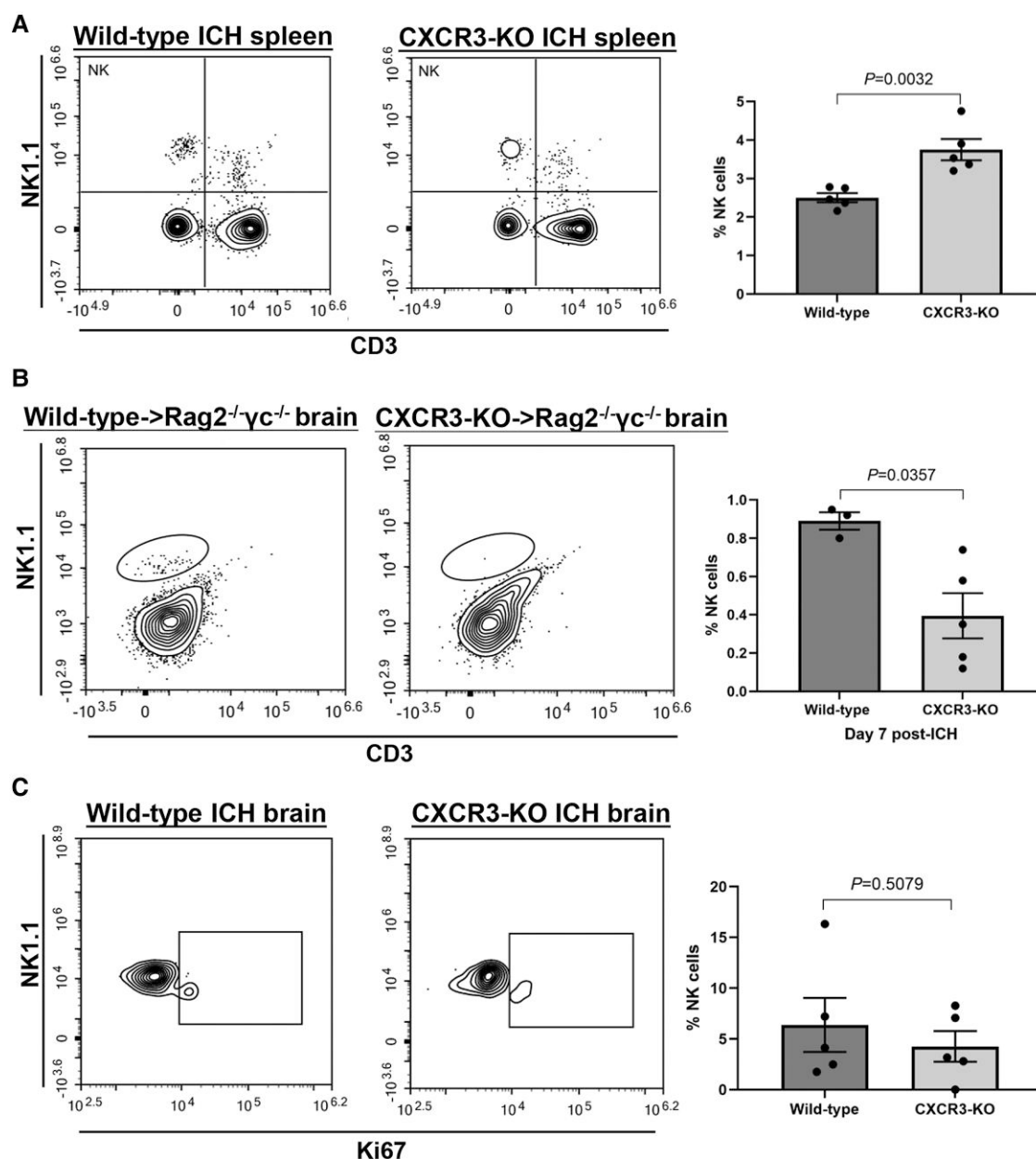
Figure 3 CXCR3 promotes the recruitment of NK cells into the haemorrhagic hemisphere from the systemic compartment. (A) A higher frequency of NK cells in the CXCR3-KO spleens was detected in comparison to that of WT spleens on Day 7 post-ICH. Flow cytometry contour plots showing populations of leucocytes in the spleens 7 days post-ICH, which were classified based on CD3 and NK1.1 surface expressions. The frequency was counted as per 100 CD45^{hi} leucocytes. $n = 5$ mice per group. Cohen's $d = 2.63$. Data are presented as mean ± standard error of the mean (SEM). Statistical significance was determined by Student's two-tailed unpaired t-test. **(B)** NK1.1$^+$ NK cells were extracted and sorted from the spleens of WT or CXCR3-KO mice and injected to each Rag2$^{-/-}$γc$^{-/-}$ mouse intravenously 3 days after ICH induction. The NK cells present in the haemorrhagic hemispheres of recipient Rag2$^{-/-}$γc$^{-/-}$ mice were from the donor mice. All NK cells in the right hemisphere were counted by flow cytometry. The percentage of WT NK cells was significantly higher than that of CXCR3-KO NK cells. $n = 3$–5 mice per group. Cohen's $d = 2.27$. Data are presented as the mean ± SEM. Statistical significance was determined by the Mann–Whitney U-test. **(C)** No statistical difference in the frequencies of NK cells expressing the proliferative marker Ki67 between the WT and CXCR3-KO groups was detected in the brain after ICH. All NK cells in the right hemisphere were counted by flow cytometry. $n = 5$ mice per group. Cohen's $d = 0.68$. Data are presented as the mean ± SEM. Statistical significance was determined by Student's two-tailed unpaired t-test. CD3 = cluster of differentiation 3; CXCR3 = CXC chemokine receptor 3; ICH = intracerebral haemorrhage; Ki67 = Kiel 67; KO = knockout; NK = natural killer; NK1.1 = killer cell lectin-like receptor subfamily B member 1A; WT = wild-type.

site was unclear. The present study demonstrated, for the first time, the role of CXCR3 in mediating NK cell recruitment in ICH. The whole concept of this study is summarized in Fig. 6.

The greater accumulation of CXCR3$^+$ NK cells in WT mice than in CXCR3-KO mice indicates a CXCR3-mediated recruitment mechanism,[50] which was probably accompanied by *de novo* synthesis of

CXCR3 after ligand binding and complex internalization.[51-54] These changes are preceded by an upregulation of CXCL10 expression that points to a site-specific migration of CXCR3$^+$ NK cells subsequent to the release of CXCL10 by the haemorrhagic brain. Our findings are consistent with previous reports concerning the role of CXCR3 in neurological diseases,[55] the upregulation of CXCL10
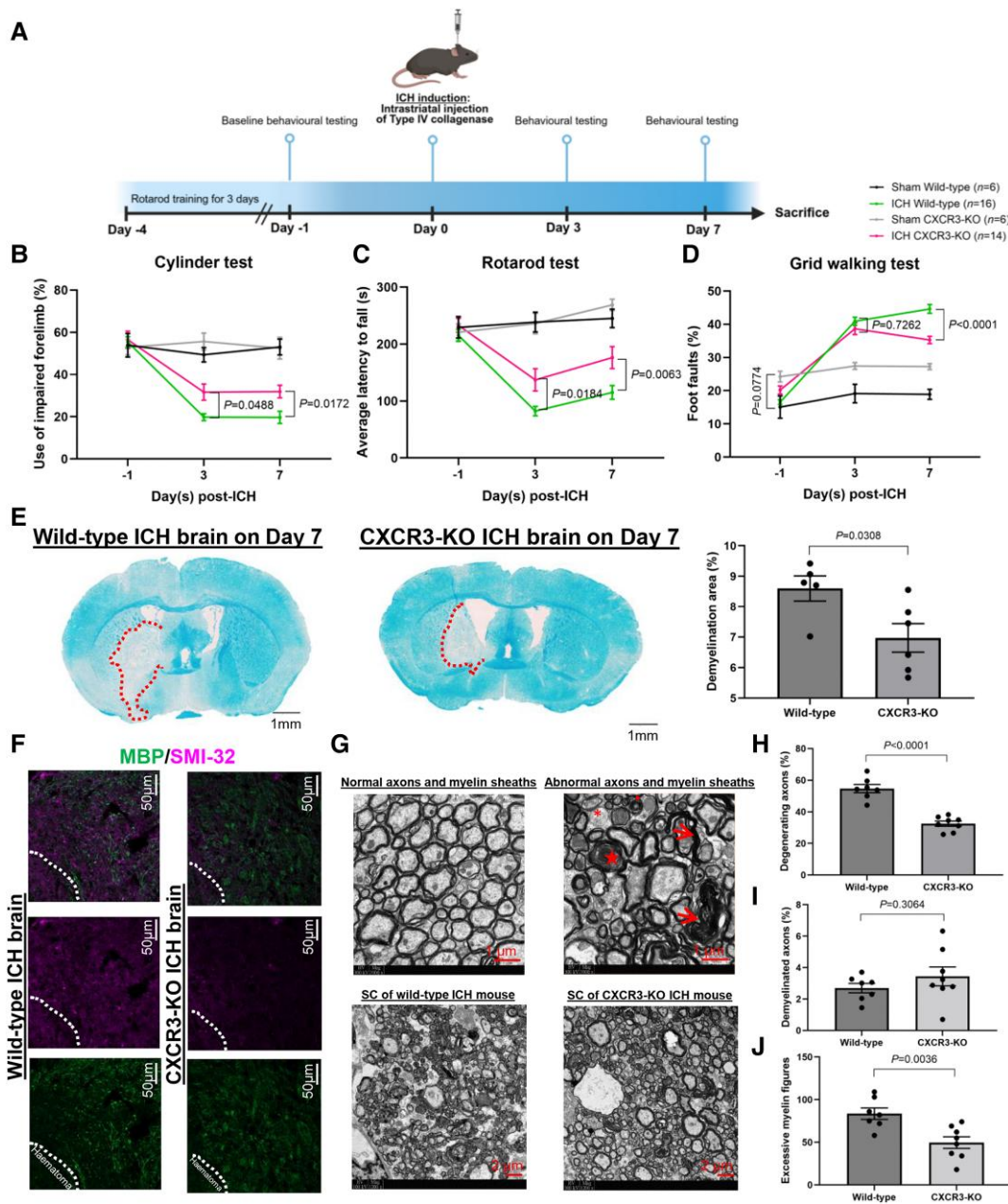
Figure 4 Global CXCR3 deficiency attenuates neurological deficits and white matter injury. (**A**) The time line of ICH induction and behavioural testing. The figures were created in BioRender. Ng, A. (2025) https://BioRender.com/j23z428. (**B**) The CXCR3-KO group had higher percentages of impaired limb usage, particularly on Day 7 (Cohen's f = 0.845). (**C**) The CXCR3-KO mice had significantly longer average latency to fall from the rotarod on Days 3 and 7 (Cohen's f = 1.54). (**D**) The percentage of foot fault was significantly lower in the CXCR3-KO group on Day 7 (Cohen's f = 1.23). Behavioural testing used n = 6 mice for sham groups, n = 16 for the WT ICH group and n = 14 for the CXCR3-KO ICH group. Data are presented as the mean ± standard error of the mean (SEM). Statistical significance was determined by two-way ANOVA followed by *post hoc* Tukey's multiple comparisons test. (**E**) Representative images at low magnification (×10) showing LFB staining of WT mouse brain and CXCR3-KO mouse brain 7 days after ICH. The pale demyelinated area is indicated by a red dotted line on each image. The CXCR3-KO group had a significantly smaller demyelinated area than the WT group. n = 5–6 mice per group. Cohen's d = 1.55. Data are presented as the mean ± SEM. Statistical significance was determined by Student's two-tailed unpaired t-test. (**F**) Representative images of immunofluorescence staining of MBP in red taken in the peri-haematomal region at low magnification (×20) illustrating the staining intensity of WT and CXCR3-KO brains on Day 7 post-ICH. A lower intensity level of SMI-32 and a higher intensity level of MBP were observed in KO mice. The edge of the haematoma on each image is delineated by a white dotted line. CXCR3-KO mice had better structural integrity of white matter. (**G**) Electron micrographs showing the ultrastructure of axons and myelin sheaths at higher magnification (×1200 and ×3900). Healthy CST axons are being wrapped in compact myelin sheaths at spinal cord C5 level from sham animals at ×3900. Examples of white matter pathologies are a demyelinated axon (red star), dark generation of axon being wrapped by loose myelin sheath lamellae (red asterisk), swollen mitochondrion (red arrowhead) and excessive myelin figures (red arrow) at spinal cord C5 level from ICH animals at ×3900. Representative images at ×1200 show axonal degeneration and myelin sheath abnormalities in the CST within the cervical spinal cord at C5 level (SC) on Day 7 post-ICH. (**H–J**) Quantification of white matter abnormalities in the CST at C5 level via the percentage of degenerating axons (Cohen's d = 3.83) (**H**), the percentage of demyelinated axon (Cohen's d = 0.89) (**I**) and counting the number of excessive myelin figures (Cohen's d = 1.83) (**J**). The white matter structures were partly preserved in the KO mice. n = 7–8 mice per ICH group. Data are presented as the mean ± SEM. Statistical significance was determined by Student's two-tailed unpaired t-test. CST = corticospinal tract; ICH = intracerebral haemorrhage; CXCR3 = CXC chemokine receptor 3; KO = knockout; LFB = Luxol Fast Blue; MBP = myelin basic protein; s = seconds; SC = spinal cord; SMI-32 = anti-neurofilament H (non-phosphorylated) antibody; NK = natural killer; WT = wild-type.
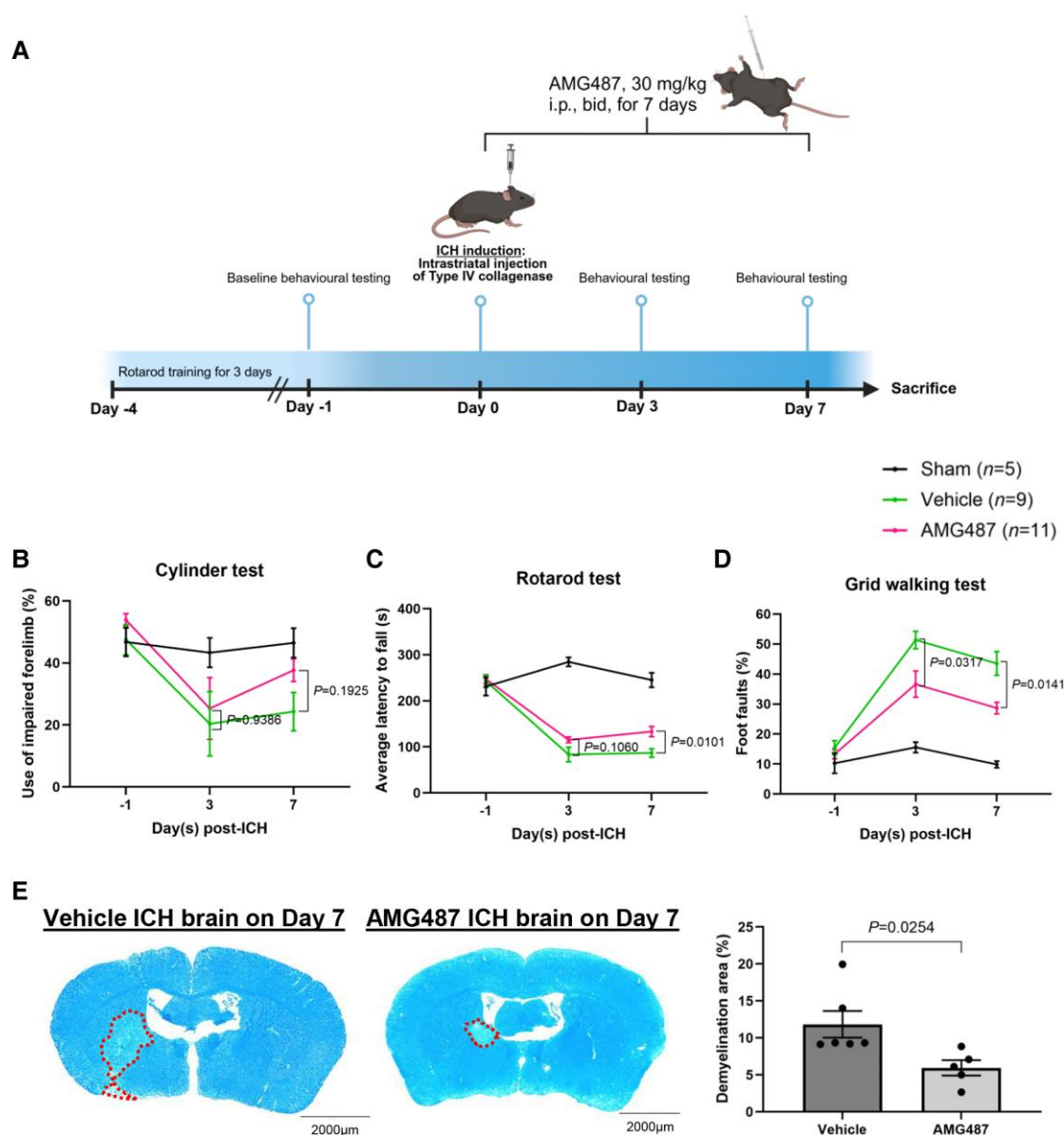
Figure 5 Systemic CXCR3 antagonism by AMG487 improved outcomes of ICH. (A) The time line of ICH induction, behavioural testing and drug administration. The figures were created in BioRender. Ng, A. (2025) https://BioRender.com/l40f433. **(B)** The treatment group had a higher percentage of impaired limb usage on Day 7 despite not reaching statistical significance (Cohen's $f = 1.75$). **(C)** The mice receiving AMG487 treatment had significantly longer average latency to fall on Day 7 (Cohen's $f = 0.612$). **(D)** The percentage of foot fault was significantly lower in the AMG487 group on Day 3 and Day 7 after ICH (Cohen's $f = 1.16$). Behavioural testing used $n = 5$ mice for the sham group, $n = 9$ for the vehicle group and $n = 11$ for the treatment group. Data are presented as the mean ± standard error of the mean (SEM). Statistical significance was determined by two-way ANOVA followed by *post hoc* Tukey's multiple comparisons test. **(E)** Representative images at low magnification (×10) showing LFB staining of vehicle group and AMG487 group 7 days after ICH. The pale demyelinated area is indicated by a red dotted line on each image. The AMG487 group had a significantly smaller demyelinated area than the vehicle group (Cohen's $d = 1.62$). $n = 5$–6 mice per group. Data are presented as mean ± SEM. Statistical significance was determined by Student's two-tailed unpaired *t*-test. bid = twice daily; i.p. = intraperitoneal; ICH = intracerebral haemorrhage; LFB = Luxol Fast Blue; s = seconds.

in the serum of ICH patients,[23] the association between high CXCL10 serum levels and poorer patient outcomes,[23] and the postulation that the CXCL10–CXCR3 axis is detrimental to the host in sterile neuroinflammation.[56]

We also found that IFN-γ⁺ NK cells were recruited by a CXCR3-dependent mechanism in this ICH model. Although the pathogenic roles of different subsets of NK cells in neurological conditions have not been characterized thoroughly,[21,57-59] it is widely accepted that their recruitment to the brain is generally coordinated by specific surface markers and their ligands.[11,60-65] Moreover, IFN-γ is one of the major downstream effectors released

by CXCR3-expressing cells, including NK cells,[60,62,63,66,67] and CXCR3 signalling has been shown to influence IFN-γ production by T cells.[57,68-70] All these suggest a close association between CXCR3 and IFN-γ. Previous studies demonstrated that IFN-γ participates in white matter injury as a pro-inflammatory cytokine in ICH,[11,21,64,65,71-73] and that both NK cells and IFN-γ can cause white matter injury in neurological diseases and in ageing white matter.[13,61,63,74-78] Of note, this study focused on the mechanism underlying the recruitment of NK cells but did not confirm the role of IFN-γ in NK cell-mediated white matter injury in ICH. Further research on the linkage between IFN-γ, NK cells and CXCR3 in ICH is warranted.
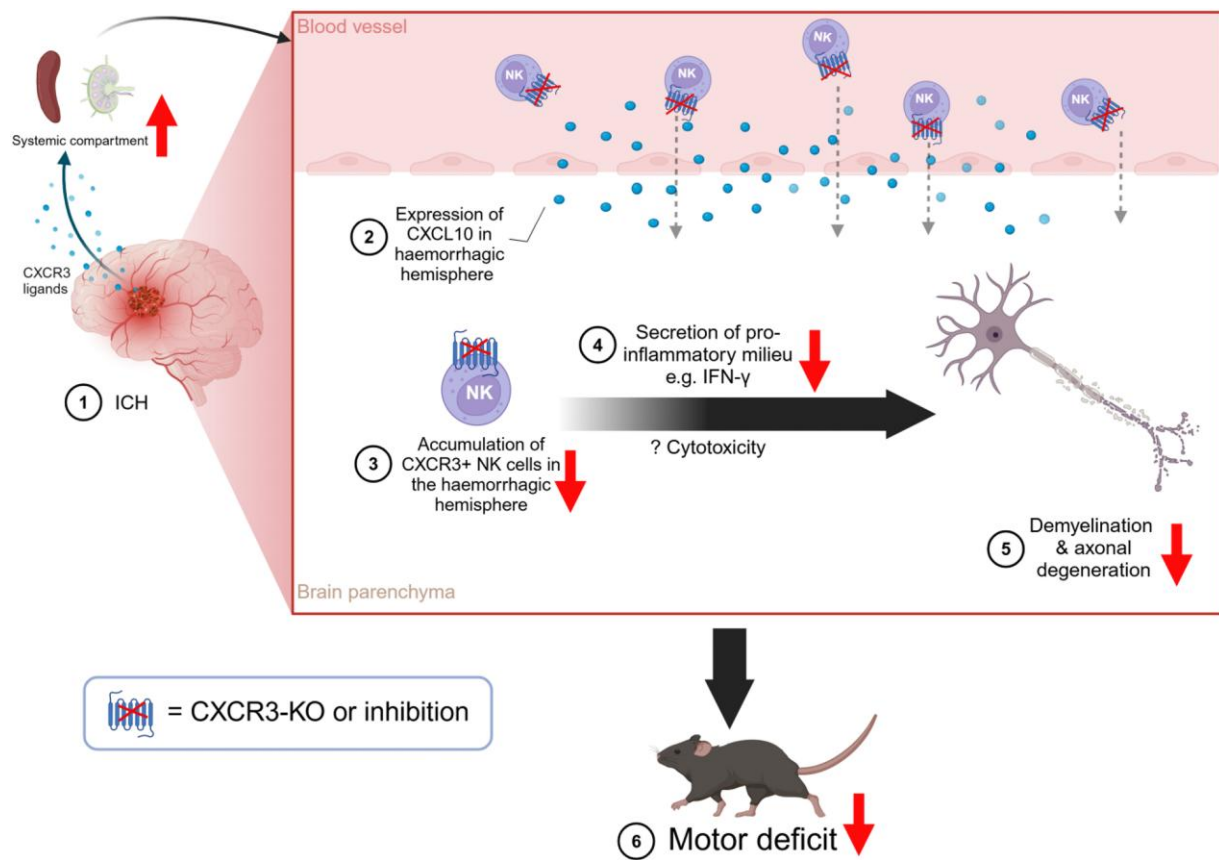
Figure 6 A graphical summary. (**1** and **2**) ICH upregulated the expression of CXCL10, a CXCR3 ligand, in the haemorrhagic hemisphere for ≥1 week. CXCR3-expressing NK cells enter the lesioned hemisphere from a systemic compartment, such as the spleen, in response to ligands released by haemorrhagic brain. (**3** and **4**) After arriving at the lesion site, CXCR3-expressing NK cells aggravated white matter injury via secretion of pro-inflammatory cytokines, such as IFN-γ, and/or direct cytotoxicity to cells. (**5** and **6**) White matter injury ultimately contributed to the motor deficit, which was reflected by behavioural test results. Genetic depletion or antagonism of CXCR3 (red crosses) resulted in a significant decrease in the accumulation of NK cells in the haemorrhagic hemisphere, less IFN-γ production, a milder degree of white matter injury and motor deficits (red arrows pointing downwards) and a concomitant increase in the frequency of NK cells in the systemic compartment (a red arrow pointing upwards). This diagram was created in BioRender. Ng, A. (2025) https://BioRender.com/b10s462 and adapted from Waldman, A. (2022) BioRender. CXCR3 = CXC chemokine receptor 3; CXCL10 = CXC motif chemokine ligand 10; ICH = intracerebral haemorrhage; IFN-γ = interferon-gamma; NK = natural killer.

The mechanism through which IFN-γ$^+$ NK cells cause such injuries in human subjects is less clear. Although CD56^{bright} NK cells, the main subset of human CXCR3-carrying NK cells, have been shown to possess greater cytokine secretion ability but less cytotoxic potential than non-CXCR3-carrying CD56^{dim} cells,[79,80] their murine CXCR3$^+$ counterparts might behave differently,[57,68] as demonstrated by in vitro co-culture experiments showing direct cytotoxicity of NK cells to CNS resident cells.[61] Cell types expressing ligands for NK cell activation, such as oligodendrocytes and neurons, are particularly susceptible to NK cell killing.[61] Whether CXCR3$^+$ NK cells mediate subsequent white matter injury via cytokine production and/or direct killing in human ICH requires further investigations.[79,80] Nevertheless, CXCR3, NK cells and IFN-γ secretion are commonly engaged in a positive feedback loop in the type I inflammatory response, which is likely to account for our observations.[81,82]

NK cell accumulation in the present context is more likely to be the result of CXCR3-mediated recruitment from the systemic compartment rather than local expansion within the haemorrhagic hemisphere. Marquardt et al.[20] previously reported an association between CXCR3 expression and NK cell proliferative capacity in vitro, but it was unclear whether the former was merely a bystander marker of cellular proliferation. We did not find a significant difference in the percentage of Ki67$^+$ NK cells between the WT and CXCR3-KO groups, which argues against CXCR3-induced local proliferation. On the contrary, we surmise that CXCR3 might induce NK cell homing towards the CNS from the spleen.[22,61,81,83-85] More NK cells were found within the spleen and fewer were located within the haemorrhagic brain in CXCR3-KO mice when compared with WT mice, which suggests a failure of ingress from the systemic compartment to the brain. By means of adoptive transfer of splenic NK cells obtained from WT or CXCR3-KO mice into Rag2$^{-/-}$γc$^{-/-}$ mice, which lack NK cells, we confirmed that active NK cell trafficking into the haemorrhagic hemisphere is CXCR3 dependent in mice, at least during the first week after ICH. Whether the same occurs in humans is unclear, although NK cells have been shown to be more abundant within the intracerebral haematoma than in the peripheral blood of ICH patients.[2,4]

The temporal profile of NK cell recruitment also appears to be important. According to the observations by Li et al.,[5] most human NK cells that entered the haemorrhagic brain within the first 12 h were CD56^{dim} that did not express a high level of CXCR3 without the appropriate triggers[71,72]; much less is known about the response of CXCR3-expressing CD56^{bright} NK cells in subsequent phases of ICH, when they might exhibit greater migratory capacity than other NK cell subsets.[2,5,86] CD56^{bright} NK cells might be less susceptible than CD56^{dim} NK cells to cell death secondary to oxygen radicals produced by neutrophils.[87] We therefore surmise that although acute

blood–brain barrier disruption post-ICH would enable the ingress of different NK cell subsets to the lesion site, more CXCR3^{+}CD56^{bright} NK cells are recruited later by means of chemokine release, and they might survive longer as secondary bran injury progresses with the generation of oxidative stress.[68] Further research is required to confirm this.

The present study showed that CXCR3 deficiency/inhibition would suppress neuroinflammation and attenuate secondary brain injury post-ICH. CXCR3-KO mice, with reduced cerebral accumulation of IFN-γ^{+} NK cells, exhibited better motor functions and less pronounced white matter injury than did WT mice. The fact that AMG487, a CXCR3 antagonist, was able to improve functional recovery further highlights the translational significance of our findings. The altered NK cell response to experimental ICH in animals with systemic CXCR3 deficiency is most probably a disease-specific phenomenon rather than the result of overall NK cell deficiency,[88,89] as demonstrated by previous studies reporting no NK cell deficiency in the systemic compartment in the absence of CXCR3.[90-93] Regarding the pathogenic significance of this relatively small population of NK cells in the haemorrhagic hemisphere, it has been demonstrated that unrestrained peripheral leucocyte infiltration is detrimental to brain parenchyma, which is normally devoid of peripheral immune cells.[79] Furthermore, NK cells might recruit additional neutrophils,[5] and a small number of NK cells might interact with multiple target cells over time to cause significant secondary injury.[94] Dysregulated inflammatory processes, such as microglia/macrophage activation by IFN-γ, might further exacerbate brain injury in ICH.[95]

An interesting observation in our study is that CXCR3 did not modulate the CD3^{+} T cell response. In line with previous studies, CXCR3 was detected on CD3^{+} T cells after ICH in our model (data not shown), but this was not accompanied by any altered CD3^{+} T cell response (data not shown), consistent with previous reports.[20,70-72,96] It is plausible that compensatory mechanisms independent of CXCR3 signalling might have stepped in to maintain the T cell response.[97] Furthermore, although CXCR3 can be highly expressed by activated CD4^{+} T helper 1 cells, a subset of CD3^{+} T cells that participates in the inflammatory response,[27,98-100] their significance during the first week post-ICH, when a full adaptive response is not yet mounted, could be less pronounced.[101,102] Notwithstanding, our results suggest that CXCR3 signalling is probably not crucial for mounting a T-cell response in experimental ICH; further research is needed. Besides, a biphasic pattern of CXCL10 expression was observed in this study. It is known that CXCL10 can be induced by a wide range of stimuli in multiple cell types.[52] Literature supports the capability of CNS resident cells, including astrocytes, neurons, microglia, endothelial cells and oligodendrocytes, to express CXCR3 ligands.[56,103-105] Human CSF contains minimal levels of CXCR3 ligands in physiological or non-inflammatory conditions, which can be greatly induced by CNS insults.[106-108] In neurological diseases with substantial involvement of peripheral leucocytes, the secretion of CXCR3 ligands by resident cells recruit leucocytes to the CNS, resulting in another bout of CXCR3 ligand production.[109] Multiple cytokines, including IFN-γ, that can induce CXCL10 expression are under the control of innate immune response.[110-112] In particular, IFN-γ forms a positive feedback loop with the CXCR3 system by triggering CXCL10 expression to attract CXCR3^{+} leucocytes, which are the main producers of IFN-γ in inflamed tissues.[82,113] Hence, the biphasic pattern of CXCL10 expression could be attributable to initial CXCL10 production by CNS resident cells after ICH, which is followed by the amplification of CXCL10 signals by CXCR3^{+} innate immune cells.

The present study has several limitations. First, the use of adult male mice might not entirely reflect the physiological response of CXCR3 system in middle-aged and elderly humans, because it is a condition of age. Additionally, the gene encoding for CXCR3 is in the chromosome X in both humans and mice, suggesting that the magnitude of CXCR3-mediated response might differ between males and females.[27] Further studies using aged and female mice should be performed to confirm the role of CXCR3 in ICH. Second, the intrinsic limitations of C57BL/6 mice precluded a complete analysis of the CXCR3 system, because neither WT nor CXCR3-KO mice have functional CXCL11 and endogenous CXCL11–CXCR3 axis,[114,115] and CXCL11 could, potentially, have opposed the effects of CXCL9 and CXCL10.[116-118] Therefore, other mouse strains should be used to examine the functional importance of CXCL11–CXCR3 signalling. Third, the only CXCR3 isoform present in mice is CXCR3-A, whereas two other isoforms, CXCR3-B and CXCR3-alt, are also found in humans.[24,119] CXCR3-A is the main CXCR3 isoform examined in an array of diseases, including neurological diseases, but only scarce information on CXCR3-B and CXCR3-alt is available.[120] In future, specimens obtained from ICH patients might be used to examine different CXCR3 isoforms and to verify our results. Fourth, we focused mainly on the therapeutic potential of CXCR3 inhibition instead of a detailed assessment of NK cell response in ICH. More detailed mechanistic studies, including the use of NK-specific CXCR3KO mice and conditional KO mice, are necessary to support clinical translation. Fifth, no CXCR3 antagonist has yet been approved for clinical use.[24] Although we have shown that a disruption of the interactions between CXCR3-A and its ligands, CXCL9 and CXCL10, is potentially beneficial, chemokine receptor antagonists might fail to achieve the intended therapeutic effects, because ligands might preferentially activate specific downstream pathways after binding, a concept known as ligand bias.[121,122] To realize the translation potential of our findings, the optimal therapeutic agent should be so designed as to specifically intervene with the binding of CXCL10 and/or CXCL9 to CXCR3 and the subsequent downstream pathway.[123,124]

Conclusion

This study is the first to delineate the mechanism of action underlying NK cell recruitment to the haemorrhagic brain, in addition to the therapeutic potential of CXCR3 antagonism in mitigating the progression of secondary brain injury and in improving functional outcome after ICH. Future research might examine the functional importance of CXCL11–CXCR3 signalling, the role of CXCR3 in mediating the production of IFN-γ and subsequent white matter injury in human ICH, and the role of different CXCR3 isoforms. Systemic CXCR3 inhibition is a potentially feasible and effective therapeutic approach for ICH that deserves further exploration, including the development and testing of the applicable pharmacological agents.

Data availability

The data that support the findings of this study are available from the corresponding author, upon reasonable request.

Acknowledgements

Funding

Competing interests

The authors report no competing interests.

Supplementary material

Supplementary material is available at *Brain* online.

References

1. Xue M, Yong VW. Neuroinflammation in intracerebral haemorrhage: Immunotherapies with potential for translation. *Lancet Neurol*. 2020;19:1023-1032.
2. Lusk JB, Quinones QJ, Staats JS, et al. Coupling hematoma evacuation with immune profiling for analysis of neuroinflammation after primary intracerebral hemorrhage: A pilot study. *World Neurosurg*. 2022;161:162-168.
3. Mei S, Shao Y, Fang Y, et al. The changes of leukocytes in brain and blood after intracerebral hemorrhage. *Front Immunol*. 2021;12:617163.
4. Goods BA, Askenase MH, Markarian E, et al. Leukocyte dynamics after intracerebral hemorrhage in a living patient reveal rapid adaptations to tissue milieu. *JCI Insight*. 2021;6:e145857.
5. Li Z, Li M, Shi SX, et al. Brain transforms natural killer cells that exacerbate brain edema after intracerebral hemorrhage. *J Exp Med*. 2020;217:e20200213.
6. Zhao X, Ting S-M, Liu C-H, et al. Neutrophil polarization by IL-27 as a therapeutic target for intracerebral hemorrhage. *Nat Commun*. 2017;8:602.
7. Zhao X, Ting S-M, Sun G, et al. Beneficial role of neutrophils through function of lactoferrin after intracerebral hemorrhage. *Stroke*. 2018;49:1241-1247.
8. Hammond MD, Taylor RA, Mullen MT, et al. CCR2$^+$Ly6C^{hi} inflammatory monocyte recruitment exacerbates acute disability following intracerebral hemorrhage. *J Neurosci*. 2014;34:3901-3909.
9. Taylor RA, Hammond MD, Ai Y, et al. CX3CR1 signaling on monocytes is dispensable after intracerebral hemorrhage. *PLoS One*. 2014;9:e114472.
10. Hammond MD, Ai Y, Sansing LH. Gr1+ macrophages and dendritic cells dominate the inflammatory infiltrate 12 hours after experimental intracerebral hemorrhage. *Transl Stroke Res*. 2012;3:s125–ss131.
11. Rolland WB, Lekic T, Krafft PR, et al. Fingolimod reduces cerebral lymphocyte infiltration in experimental models of rodent intracerebral hemorrhage. *Exp Neurol*. 2013;241:45-55.
12. Zhang W, Wu Q, Hao S, et al. The hallmark and crosstalk of immune cells after intracerebral hemorrhage: Immunotherapy perspectives. *Front Neurosci*. 2023;16:1117999.
13. Fu X, Zhou G, Zhuang J, et al. White matter injury after intracerebral hemorrhage. *Front Neurol*. 2021;12:562090.
14. Marcet P, Santos N, Borlongan CV. When friend turns foe: Central and peripheral neuroinflammation in central nervous system injury. *Neuroimmunol Neuroinflamm*. 2017;4:82-92.
15. Bryceson YT, Chiang SCC, Darmanin S, et al. Molecular mechanisms of natural killer cell activation. *J Innate Immun*. 2011;3:216-226.
16. Feng Y, Wu Q, Zhang T, et al. Natural killer cell deficiency experiences higher risk of sepsis after critical intracerebral hemorrhage. *Int J Immunopathol Pharmacol*. 2021;35:20587384211056495.
17. Ubogu EE, Cossoy MB, Ransohoff RM. The expression and function of chemokines involved in CNS inflammation. *Trends Pharmacol Sci*. 2006;27:48-55.
18. Hughes CE, Nibbs RJB. A guide to chemokines and their receptors. *FEBS J*. 2018;285:2944-2971.
19. Yao Y, Tsirka SE. The CCL2-CCR2 system affects the progression and clearance of intracerebral hemorrhage. *Glia*. 2012;60:908-918.
20. Marquardt N, Wilk E, Pokoyski C, et al. Murine CXCR3$^+$CD27^{bright} NK cells resemble the human CD56^{bright} NK-cell population. *Eur J Immunol*. 2010;40:1428-1439.
21. Poli A, Michel T, Thérésine M, Andrès E, Hentges F, Zimmer J. CD56^{bright} natural killer (NK) cells: An important NK cell subset. *Immunology*. 2009;126:458-465.
22. Zhang Y, Gao Z, Wang D, et al. Accumulation of natural killer cells in ischemic brain tissues and the chemotactic effect of IP-10. *J Neuroinflamm*. 2014;11:79.
23. Landreneau MJ, Mullen MT, Messé SR, et al. CCL2 and CXCL10 are associated with poor outcome after intracerebral hemorrhage. *Ann Clin Transl Neurol*. 2018;5:962-970.
24. Pease JE. Designing small molecule CXCR3 antagonists. *Expert Opin Drug Discov*. 2017;12:159-168.
25. Zhang X, Han J, Man K, et al. CXC chemokine receptor 3 promotes steatohepatitis in mice through mediating inflammatory cytokines, macrophages and autophagy. *J Hepatol*. 2016;64:160-170.
26. Tu W, Zheng J, Liu Y, et al. The aminobisphosphonate pamidronate controls influenza pathogenesis by expanding a γδ T cell population in humanized mice. *J Exp Med*. 2011;208:1511-1522.
27. Oghumu S, Varikuti S, Stock JC, et al. Cutting edge: CXCR3 escapes X chromosome inactivation in T cells during infection: Potential implications for sex differences in immune responses. *J Immunol*. 2019;203:789-794.
28. Ng ACK, Yao M, Cheng SY, et al. Protracted morphological changes in the corticospinal tract within the cervical spinal cord after intracerebral hemorrhage in the right striatum of mice. *Front Neurosci*. 2020;14:506.
29. Ha Y, Liu H, Zhu S, et al. Critical role of the CXCL10/C-X-C chemokine receptor 3 axis in promoting leukocyte recruitment and neuronal injury during traumatic optic neuropathy induced by optic nerve crush. *Am J Pathol*. 2017;187:352-365.
30. Greenberg SM, Ziai WC, Cordonnier C, et al. 2022 guideline for the management of patients with spontaneous intracerebral hemorrhage: A guideline from the American Heart Association/American stroke association. *Stroke*. 2022;53:e282-e361.
31. Okauchi M, Hua Y, Keep RF, et al. Deferoxamine treatment for intracerebral hemorrhage in aged rats: Therapeutic time window and optimal duration. *Stroke*. 2010;41:375-382.
32. Liu J, Li N, Zhu Z, et al. Vitamin D enhances hematoma clearance and neurologic recovery in intracerebral hemorrhage. *Stroke*. 2022;53:2058-2068.
33. Jung K-H, Chu K, Jeong S-W, et al. HMG-CoA reductase inhibitor, atorvastatin, promotes sensorimotor recovery, suppressing acute inflammatory reaction after experimental intracerebral hemorrhage. *Stroke*. 2004;35:1744-1749.
34. Mi S, Hu B, Hahm K, et al. LINGO-1 antagonist promotes spinal cord remyelination and axonal integrity in MOG-induced experimental autoimmune encephalomyelitis. *Nat Med*. 2007;13:1228-1233.
35. Kiang KM, Zhang P, Li N, Zhu Z, Jin L, Leung GK-K. Loss of cytoskeleton protein ADD3 promotes tumor growth and angiogenesis in glioblastoma multiforme. *Cancer Lett*. 2020;474:118-126.

36. Romero-Suarez S, Del Rio Serrato A, Bueno RJ, et al. The central nervous system contains ILC1s that differ from NK cells in the response to inflammation. *Front Immunol.* 2019;10:2337.

37. Hussain RZ, Miller-Little WA, Doelger R, et al. Defining standard enzymatic dissociation methods for individual brains and spinal cords in EAE. *NeurolNeuroimmunol Neuroinflamm.* 2018;5:e437.

38. Hills LB, Abdullah L, Lust HE, Degefu H, Huang YH. Foxo1 serine 209 is a critical regulatory site of CD8 T cell differentiation and survival. *J Immunol.* 2021;206:89-100.

39. Cai W, Shi L, Zhao J, et al. Neuroprotection against ischemic stroke requires a specific class of early responder T cells in mice. *J Clin Invest.* 2022;132:e157678.

40. Faul F, Erdfelder E, Buchner A, Lang A-G. Statistical power analyses using G*power 3.1: Tests for correlation and regression analyses. *Behav Res Methods.* 2009;41:1149-1160.

41. Karbasforoushan H, Cohen-Adad J, Dewald JPA. Brainstem and spinal cord MRI identifies altered sensorimotor pathways post-stroke. *Nat Commun.* 2019;10:3524.

42. Yang J, Li Q, Wang Z, et al. Multimodality MRI assessment of grey and white matter injury and blood-brain barrier disruption after intracerebral haemorrhage in mice. *Sci Rep.* 2017;7:40358.

43. Zhang Y, Yang Y, Zhang GZ, et al. Stereotactic administration of edaravone ameliorates collagenase-induced intracerebral hemorrhage in rat. *CNS Neurosci Ther.* 2016;22:824-835.

44. Chen Z, Xu N, Dai X, et al. Interleukin-33 reduces neuronal damage and white matter injury via selective microglia M2 polarization after intracerebral hemorrhage in rats. *Brain Res Bull.* 2019;150:127-135.

45. Xia Y, Pu H, Leak RK, et al. Tissue plasminogen activator promotes white matter integrity and functional recovery in a murine model of traumatic brain injury. *Proc Natl Acad Sci U S A.* 2018;115:E9230-E9238.

46. Yandamuri SS, Lane TE. Imaging axonal degeneration and repair in preclinical animal models of multiple sclerosis. *Front Immunol.* 2016;7:189.

47. Qin D, Wang J, Le A, Wang TJ, Chen X, Wang J. Traumatic brain injury: Ultrastructural features in neuronal ferroptosis, glial cell activation and polarization, and blood–brain barrier breakdown. *Cells.* 2021;10:1009.

48. Li Q, Weiland A, Chen X, et al. Ultrastructural characteristics of neuronal death and white matter injury in mouse brain tissues after intracerebral hemorrhage: Coexistence of ferroptosis, autophagy, and necrosis. *Front Neurol.* 2018;9:581.

49. Vargas ME, Barres BA. Why is Wallerian degeneration in the CNS so slow? *Annu Rev Neurosci.* 2007;30:153-179.

50. Müller M, Carter S, Hofer MJ, et al. Review: The chemokine receptor CXCR3 and its ligands CXCL9, CXCL10 and CXCL11 in neuroimmunity—A tale of conflict and conundrum. *Neuropathol Appl Neurobiol.* 2010;36:368-387.

51. Meiser A, Mueller A, Wise EL, et al. The chemokine receptor CXCR3 is degraded following internalization and is replenished at the cell surface by de novo synthesis of receptor. *J Immunol.* 2008;180:6713-6724.

52. Metzemaekers M, Vanheule V, Janssens R, et al. Overview of the mechanisms that may contribute to the non-redundant activities of interferon-inducible CXC chemokine receptor 3 ligands. *Front Immunol.* 2018;8:1970.

53. Smith JS, Alagesan P, Desai NK, et al. C-X-C motif chemokine receptor 3 splice variants differentially activate beta-arrestins to regulate downstream signaling pathways. *Mol Pharmacol.* 2017;92:136-150.

54. Colvin RA, Campanella GSV, Sun J, et al. Intracellular domains of CXCR3 that mediate CXCL9, CXCL10, and CXCL11 function. *J Biol Chem.* 2004;279:30219-30227.

55. Zhou Y-Q, Liu DQ, Chen SP, et al. The role of CXCR3 in neurological diseases. *Curr Neuropharmacol.* 2019;17:142-150.

56. McKimmie C, Michlmayr D. Role of CXCL10 in central nervous system inflammation. *Int J Interferon Cytokine Mediat Res.* 2014;6:1-18.

57. Chiossone L, Chaix J, Fuseri N, Roth C, Vivier E, Walzer T. Maturation of mouse NK cells is a 4-stage developmental program. *Blood.* 2009;113:5488-5496.

58. Gao M, Yang Y, Li D, et al. CD27 natural killer cell subsets play different roles during the pre-onset stage of experimental autoimmune encephalomyelitis. *Innate Immun.* 2016;22:395-404.

59. Kaur G, Trowsdale J, Fugger L. Natural killer cells and their receptors in multiple sclerosis. *Brain.* 2013;136:2657-2676.

60. Tirotta E, Ransohoff RM, Lane TE. CXCR2 signaling protects oligodendrocyte progenitor cells from IFN-γ/CXCL10-mediated apoptosis. *Glia.* 2011;59:1518-1528.

61. Shi Fu-Dong, Ransohoff Richard M. Chapter twenty-eight: Nature killer cells in the central nervous system. In: Thomson AW, Lotze MT, eds. *Natural killer cells.* Academic Press; 2010:373–383.

62. Peferoen L, Kipp M, Van Der Valk P, et al. Oligodendrocyte-microglia cross-talk in the central nervous system. *Immunology.* 2014;141:302-313.

63. Watzlawik J, Warrington AE, Rodriguez M. Importance of oligodendrocyte protection, BBB breakdown and inflammation for remyelination. *Expert Rev Neurother.* 2010;10:441-457.

64. Liesz A, Middelhoff M, Zhou W, Karcher S, Illanes S, Veltkamp R. Comparison of humoral neuroinflammation and adhesion molecule expression in two models of experimental intracerebral hemorrhage. *Exp Transl Stroke Med.* 2011;3:11.

65. Lu Q, Gao L, Huang L, et al. Inhibition of mammalian target of rapamycin improves neurobehavioral deficit and modulates immune response after intracerebral hemorrhage in rat. *J Neuroinflammation.* 2014;11:44.

66. King T, Lamb T. Interferon-γ: The Jekyll and Hyde of malaria. *PLoS Pathog.* 2015;11:e1005118.

67. Spencer NG, Schilling T, Miralles F, et al. Mechanisms underlying interferon-γ-induced priming of microglial reactive oxygen species production. *PLoS One.* 2016;11:e0162497.

68. Hayakawa Y, Smyth MJ. CD27 dissects mature NK cells into two subsets with distinct responsiveness and migratory capacity. *J Immunol.* 2006;176:1517-1524.

69. Xu J, Neal LM, Ganguly A, et al. Chemokine receptor CXCR3 is required for lethal brain pathology but not pathogen clearance during cryptococcal meningoencephalitis. *Sci Adv.* 2020;6:eaba2502.

70. Liu L, Huang D, Matsui M, et al. Severe disease, unaltered leukocyte migration, and reduced IFN-γ production in CXCR3−/− mice with experimental autoimmune encephalomyelitis. *J Immunol.* 2006;176:4399-4409.

71. Bernardini G, Antonangeli F, Bonanni V, et al. Dysregulation of chemokine/chemokine receptor axes and NK cell tissue localization during diseases. *Front Immunol.* 2016;7:402.

72. Lima M, Leander M, Santos M, et al. Chemokine receptor expression on normal blood CD56+ NK-cells elucidates cell partners that comigrate during the innate and adaptive immune responses and identifies a transitional NK-cell population. *J Immunol Res.* 2015;2015:839684.

73. Huntington ND, Vosshenrich CAJ, Di Santo JP. Developmental pathways that generate natural-killer-cell diversity in mice and humans. *Nat Rev Immunol.* 2007;7:703-714.

74. Saikali P, Antel JP, Newcombe J, et al. NKG2D-mediated cytotoxicity toward oligodendrocytes suggests a mechanism for tissue injury in multiple sclerosis. *J Neurosci.* 2007;27:1220-1228.

75. Ahmed SM, Fransen NL, Touil H, et al. Accumulation of meningeal lymphocytes correlates with white matter lesion activity in progressive multiple sclerosis. *JCI Insight*. 2022;7:e151683.

76. Sen T, Saha P, Gupta R, et al. Aberrant ER stress induced neuronal-IFNβ elicits white matter injury due to microglial activation and T-cell infiltration after TBI. *J Neurosci*. 2020;40:424-446.

77. Tao CY, Hu X, Li H, et al. White matter injury after intracerebral hemorrhage: Pathophysiology and therapeutic strategies. *Front Hum Neurosci*. 2017;11:422.

78. Kaya T, Mattugini N, Liu L, et al. CD8⁺ T cells induce interferon-responsive oligodendrocytes and microglia in white matter aging. *Nat Neurosci*. 2022;25:1446-1457.

79. Deczkowska A, Baruch K, Schwartz M. Type I/II interferon balance in the regulation of brain physiology and pathology. *Trends Immunol*. 2016;37:181-192.

80. Tschoe C, Bushnell CD, Duncan PW, et al. Neuroinflammation after intracerebral hemorrhage and potential therapeutic targets. *J Stroke*. 2020;22:29-46.

81. Bernardini G, Gismondi A, Santoni A. Chemokines and NK cells: Regulators of development, trafficking and functions. *Immunol Lett*. 2012;145:39-46.

82. Annunziato F, Romagnani C, Romagnani S. The 3 major types of innate and adaptive cell-mediated effector immunity. *J Allergy Clin Immunol*. 2015;135:626-635.

83. Grégoire C, Chasson L, Luci C, et al. The trafficking of natural killer cells. *Immunol Rev*. 2007;220:169-182.

84. Thapa M, Welner RS, Pelayo R, et al. CXCL9 and CXCL10 expression are critical for control of genital herpes simplex virus type 2 infection through mobilization of HSV-specific CTL and NK cells to the nervous system. *J Immunol*. 2008;180:1098-1106.

85. Trifilo MJ, Montalto-Morrison C, Stiles LN, et al. CXC chemokine ligand 10 controls viral infection in the central nervous system: Evidence for a role in innate immune response through recruitment and activation of natural killer cells. *J Virol*. 2004;78:585-594.

86. Gross CC, Schulte-Mecklenbeck A, Rünzi A, et al. Impaired NK-mediated regulation of T-cell activity in multiple sclerosis is reconstituted by IL-2 receptor modulation. *Proc Natl Acad Sci U S A*. 2016;113:E2973-E2982.

87. Harlin H, Hanson M, Johansson CC, et al. The CD16⁻CD56ᵇʳⁱᵍʰᵗ NK cell subset is resistant to reactive oxygen species produced by activated granulocytes and has higher antioxidative capacity than the CD16⁺CD56ᵈⁱᵐ subset. *J Immunol*. 2007;179:4513-4519.

88. Jiang D, Liang J, Hodge J, et al. Regulation of pulmonary fibrosis by chemokine receptor CXCR3. *J Clin Invest*. 2004;114:291-299.

89. Liu C, Luo D, Reynolds BA, et al. Chemokine receptor CXCR3 promotes growth of glioma. *Carcinogenesis*. 2011;32:129-137.

90. Herzig DS, Driver BR, Fang G, Toliver-Kinsky TE, Shute EN, Sherwood ER. Regulation of lymphocyte trafficking by CXC chemokine receptor 3 during septic shock. *Am J Respir Crit Care Med*. 2012;185:291-300.

91. Kohlmeier JE, Cookenham T, Miller SC, et al. CXCR3 directs antigen-specific effector CD4⁺ T cell migration to the lung during parainfluenza virus infection. *J Immunol*. 2009;183:4378-4384.

92. Steinmetz OM, Turner J-E, Paust H-J, et al. CXCR3 mediates renal Th1 and Th17 immune response in murine lupus nephritis. *J Immunol*. 2009;183:4693-4704.

93. Panzer U, Steinmetz OM, Paust H-J, et al. Chemokine receptor CXCR3 mediates T cell recruitment and tissue injury in nephrotoxic nephritis in mice. *J Am Soc Nephrol*. 2007;18:2071-2084.

94. Vanherberghen B, Olofsson PE, Forslund E, et al. Classification of human natural killer cells based on migration behavior and cytotoxic response. *Blood*. 2013;121:1326-1334.

95. Gimsa U, ØRen A, Pandiyan P, et al. Astrocytes protect the CNS: Antigen-specific T helper cell responses are inhibited by astrocyte-induced upregulation of CTLA-4 (CD152). *J Mol Med*. 2004;82:364-372.

96. Abron JD, Singh NP, Murphy AE, et al. Differential role of CXCR3 in inflammation and colorectal cancer. *Oncotarget*. 2018;9:17928-17936.

97. Sporici R, Issekutz TB. CXCR3 blockade inhibits T-cell migration into the CNS during EAE and prevents development of adoptively transferred, but not actively induced, disease. *Eur J Immunol*. 2010;40:2751-2761.

98. Dufour JH, Dziejman M, Liu MT, Leung JH, Lane TE, Luster AD. IFN-γ-inducible protein 10 (IP-10; CXCL10)-deficient mice reveal a role for IP-10 in effector T cell generation and trafficking. *J Immunol*. 2002;168:3195-3204.

99. Rosenblum JM, Zhang Q-W, Siu G, et al. CXCR3 antagonism impairs the development of donor-reactive, IFN-γ-producing effectors and prolongs allograft survival. *Transplantation*. 2009;87:360-369.

100. Karin N. Chemokines and cancer: New immune checkpoints for cancer therapy. *Curr Opin Immunol*. 2018;51:140-145.

101. Yang H, Gao X, Xiao W, et al. Minocycline alleviates white matter injury following intracerebral hemorrhage by regulating CD4⁺ T cell differentiation via notch1 signaling pathway. *Oxid Med Cell Longev*. 2022;2022:3435267.

102. Zhang X, Liu W, Yuan J, et al. T lymphocytes infiltration promotes blood-brain barrier injury after experimental intracerebral hemorrhage. *Brain Res*. 2017;1670:96-105.

103. Campanella GSV, Tager AM, El Khoury JK, et al. Chemokine receptor CXCR3 and its ligands CXCL9 and CXCL10 are required for the development of murine cerebral malaria. *Proc Natl Acad Sci U S A*. 2008;105:4814-4819.

104. Choi SS, Lee HJ, Lim I, Satoh J-I, Kim SU. Human astrocytes: Secretome profiles of cytokines and chemokines. *PLoS One*. 2014;9:e92325.

105. Hamby ME, Coppola G, Ao Y, Geschwind DH, Khakh BS, Sofroniew MV. Inflammatory mediators alter the astrocyte transcriptome and calcium signaling elicited by multiple G-protein-coupled receptors. *J Neurosci*. 2012;32:14489-14510.

106. De Laere M, Berneman ZN, Cools N. To the brain and back: Migratory paths of dendritic cells in multiple sclerosis. *J Neuropathol Exp Neurol*. 2018;77:178-192.

107. Kothur K, Bandodkar S, Wienholt L, et al. Etiology is the key determinant of neuroinflammation in epilepsy: Elevation of cerebrospinal fluid cytokines and chemokines in febrile infection-related epilepsy syndrome and febrile status epilepticus. *Epilepsia*. 2019;60:1678-1688.

108. Sato T, Coler-Reilly A, Utsunomiya A, et al. CSF CXCL10, CXCL9, and neopterin as candidate prognostic biomarkers for HTLV-1-associated myelopathy/tropical spastic paraparesis. *PLoS Negl Trop Dis*. 2013;7:e2479.

109. Satarkar D, Patra C. Evolution, expression and functional analysis of CXCR3 in neuronal and cardiovascular diseases: A narrative review. *Front Cell Dev Biol*. 2022;10:882017.

110. Groom JR, Luster AD. CXCR3 in T cell function. *Exp Cell Res*. 2011;317:620-631.

111. Honda K, Yanai H, Takaoka A, Taniguchi T. Regulation of the type I IFN induction: A current view. *Int Immunol*. 2005;17:1367-1378.

112. Loos T, Dekeyzer L, Struyf S, et al. TLR ligands and cytokines induce CXCR3 ligands in endothelial cells: Enhanced CXCL9 in autoimmune arthritis. *Lab Invest*. 2006;86:902-916.

113. Liu YQ, Poon RT, Hughes J, Li Q-Y, Yu W-C, Fan S-T. Desensitization of T lymphocyte function by CXCR3 ligands

in human hepatocellular carcinoma. *World J Gastroenterol*. 2005;11:164-170.

114. Karin N. CXCR3 ligands in cancer and autoimmunity, chemoattraction of effector T cells, and beyond. *Front Immunol*. 2020;11:976.

115. Groom JR, Luster AD. CXCR3 ligands: Redundant, collaborative and antagonistic functions. *Immunol Cell Biol*. 2011;89:207-215.

116. Karin N, Wildbaum G, Thelen M. Biased signaling pathways via CXCR3 control the development and function of CD4^{+} T cell subsets. *J Leukoc Biol*. 2016;99:857-862.

117. Yao Y, Vent-Schmidt J, McGeough MD, et al. Tr1 cells, but not Foxp3^{+} regulatory T cells, suppress NLRP3 inflammasome activation via an IL-10–dependent mechanism. *J Immunol*. 2015;195:488-497.

118. Zohar Y, Wildbaum G, Novak R, et al. CXCL11-dependent induction of FOXP3-negative regulatory T cells suppresses autoimmune encephalomyelitis. *J Clin Invest*. 2014;124:2009-2022.

119. Bakheet SA, Alrwashied BS, Ansari MA, et al. CXC chemokine receptor 3 antagonist AMG487 shows potent anti-arthritic effects on collagen-induced arthritis by modifying B cell inflammatory profile. *Immunol Lett*. 2020;225:74-81.

120. Balan M, Pal S. A novel CXCR3-B chemokine receptor-induced growth-inhibitory signal in cancer cells is mediated through the regulation of Bach-1 protein and nrf2 protein nuclear translocation. *J Biol Chem*. 2014;289:3126-3137.

121. Steen A, Larsen O, Thiele S, Rosenkilde MM. Biased and G protein-independent signaling of chemokine receptors. *Front Immunol*. 2014;5:277.

122. Proudfoot AEI. Chemokine receptors: Multifaceted therapeutic targets. *Nat Rev Immunol*. 2002;2:106-115.

123. Smith JS, Lefkowitz RJ, Rajagopal S. Biased signalling: From simple switches to allosteric microprocessors. *Nat Rev Drug Discov*. 2018;17:243-260.

124. Zheng K, Smith JS, Eiger DS, et al. Biased agonists of the chemokine receptor CXCR3 differentially signal through Gαi:β-arrestin complexes. *Sci Signal*. 2022;15:eabg5203.

This promotional article is authored and funded by Biogen.
This material is intended for UK and IE healthcare professionals only.

Prescribing Information

TYSABRI™
(natalizumab)
SUBCUTANEOUS USE | 300mg

Efficacy made Convenient

TYSABRI SC injection with the potential to administer **AT HOME** for eligible patients*

Efficacy and safety profile comparable between TYSABRI IV and SC†[1,2]

†Comparable PK, PD, efficacy, and safety profile of SC to IV except for injection site pain.[1,2]

CLICK HERE TO DISCOVER MORE ABOUT TYSABRI SC AND THE DIFFERENCE IT MAY MAKE TO YOUR ELIGIBLE PATIENTS

Supported by

BIOGEN'S
Stratify JCV™ SERVICE

A Biogen developed and funded JCV antibody index PML risk stratification service, validated and available exclusively for patients on or considering TYSABRI.

*As of April 2024, TYSABRI SC can be administered outside a clinical setting (e.g. at home) by a HCP for patients who have tolerated at least 6 doses of TYSABRI well in a clinical setting. Please refer to section 4.2 of the SmPC.[1]

TYSABRI is indicated as single DMT in adults with highly active RRMS for the following patient groups:[1,2]

- Patients with highly active disease despite a full and adequate course of treatment with at least one DMT
- Patients with rapidly evolving severe RRMS defined by 2 or more disabling relapses in one year, and with 1 or more Gd+ lesions on brain MRI or a significant increase in T2 lesion load as compared to a previous recent MRI

Very common AEs include nasopharyngitis and urinary tract infection. Please refer to the SmPC for further safety information, including the risk of the uncommon but serious AE, PML.[1,2]

Abbreviations: AE: Adverse Event; **DMT:** Disease-Modifying Therapy; **Gd+:** Gadolinium-Enhancing; **HCP:** Healthcare Professional; **IV:** Intravenous; **JCV:** John Cunningham Virus; **MRI:** Magnetic Resonance Imaging; **PD:** Pharmacodynamic; **PK:** Pharmacokinetic; **PML:** Progressive Multifocal Leukoencephalopathy; **RRMS:** Relapsing-Remitting Multiple Sclerosis; **SC:** Subcutaneous.

References: 1. TYSABRI SC (natalizumab) Summary of Product Characteristics. **2.** TYSABRI IV (natalizumab) Summary of Product Characteristics.

Biogen®